Journal of Hazardous Materials 472 (2024) 134469

Contents lists available at ScienceDirect

Journal of Hazardous Materials

journal homepage: www.elsevier.com/locate/jhazmat

Engineering of molecularly imprinted cavity within 3D covalent organic frameworks: An innovation for enhanced extraction and removal of microcystins

Yu-Hong Tang [b], Tian-Tian Ma [b], Xu-Qin Ran [b], Yukun Yang [d], Hai-Long Qian [a,b,*], Xiu-Ping Yan [a,b,c]

[a] State Key Laboratory of Food Science and Resources, Jiangnan University, Wuxi 214122, China
[b] Institute of Analytical Food Safety, School of Food Science and Technology, Jiangnan University, Wuxi 214122, China
[c] Key Laboratory of Synthetic and Biological Colloids, Ministry of Education, School of Chemical and Material Engineering, Jiangnan University, Wuxi 214122, China
[d] School of Life Science, Shanxi University, Taiyuan 030006, China

HIGHLIGHTS

- Molecularly imprinted cavity was first engineered within 3D COF.
- 3D COF-MIP gave selective and rapid extraction of MC-LR.
- A sensitive detection method was developed for MC-LR in environmental samples.
- 3D COF-MIP exhibited superior removal of MC-LR in environmental samples.

GRAPHICAL ABSTRACT

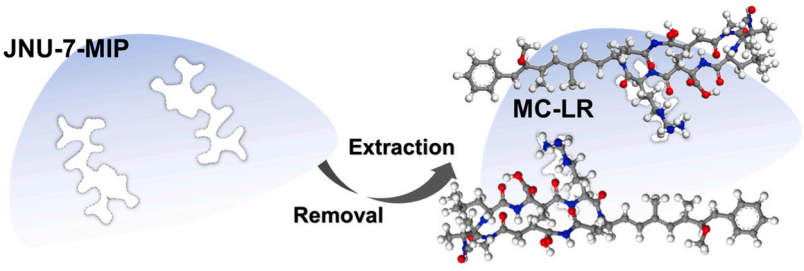

ARTICLE INFO

Keywords:
Covalent organic frameworks
Molecularly imprinted cavity
Solid-phase extraction
Removal
Microcystins

ABSTRACT

The scarcity of selective adsorbents for efficient extraction and removal of microcystins (MCs) from complex samples greatly limits the precise detection and effective control of MCs. Three-dimensional covalent organic frameworks (3D COFs), characterized by their large specific surface areas and highly ordered rigid structure, are promising candidates, but suffer from lack of specific recognition. Herein, we design to engineer molecularly imprinted cavities within 3D COFs via molecularly imprinted technology, creating a novel adsorbent with exceptional selectivity, kinetics and capacity for the efficient extraction and removal of MCs. As proof-of-concept, a new C=C bond-containing 3D COF, designated JNU-7, is designed and prepared for copolymerization with methacrylic acid, the pseudo template L-arginine and ethylene dimethacrylate to yield the JNU-7 based molecularly imprinted polymer (JNU-7-MIP). The JNU-7-MIP exhibits a great adsorption capacity (156 mg g^{-1}) for L-arginine. Subsequently, the JNU-7-MIP based solid-phase extraction coupled with high performance liquid chromatography-mass spectrometry achieves low detection limit of 0.008 ng mL^{-1}, wide linear range of 0.025–100 ng mL^{-1}, high enrichment factor of 186, rapid extraction of 10 min, and good recoveries of 92.4%–106.5% for MC-LR. Moreover, the JNU-7-MIP can rapidly remove the MC-LR from 1 mg L^{-1} to levels (0.26–0.35 μg L^{-1}) lower than the WHO recommended limit for drinking water (1 μg L^{-1}). This work reveals the

* Corresponding author at: State Key Laboratory of Food Science and Resources, Jiangnan University, Wuxi 214122, China.
E-mail address: hlqian@jiangnan.edu.cn (H.-L. Qian).

https://doi.org/10.1016/j.jhazmat.2024.134469
Received 20 February 2024; Received in revised form 25 April 2024; Accepted 27 April 2024
Available online 28 April 2024

considerable potential of 3D COF based MIPs as promising adsorbents for the extraction and removal of contaminants in complex real samples.

1. Introduction

Microcystins (MCs), a type of cyclic heptapeptide toxins produced by cyanobacterial blooms, are one of the predominant toxins in aquatic ecosystems. Prolonged and chronic exposure to MCs has been documented to be associated with various adverse health impacts on the liver, kidney, heart, reproductive systems, and lungs [1–4]. MC-LR is of primary concern due to its most prevalent existence and high toxicity among more than 100 identified MCs [5–7]. The World Health Organization (WHO) has recommended a maximum limit of 1.0 μg L^{-1} for the MC-LR in drinking water. In addition, almost all countries specify the limited concentration of the MC-LR (ranging from 1.0 to 1.5 μg L^{-1}) in drinking water [8]. Since a large number of interfering matrices exist in real samples, the application of adsorbents for pre-concentration and purification is of great significance for the detection and control of MC-LR. However, traditional adsorbents, including C8, C18 and ion-exchange materials, remain challenging in meeting the real-sample demands due to their low selectivity and capacity towards the MC-LR [9,10].

Covalent organic frameworks (COFs) are emerging crystalline polymers characterized by their large specific surface areas and highly ordered rigid structures, and have already demonstrated great potential as adsorbents for sample pre-treatment and removal [11–14]. Topology of COFs is classified into two-dimensional (2D) and three-dimensional (3D) varieties. 2D COFs, featuring solely channels, are typically formed by stacking of planar polymeric layers via non-covalent linkers [15]. In contrast, 3D COFs, consisting of stereoscopic tetrahedral monomers through pure covalent bond give more stable and accessible open sites, which are conducive to rapid interaction with targets [16,17]. Thereby, 3D COFs are promising candidates as novel adsorbents for the extraction and removal of MC-LR from complex samples, but suffer from low specific recognition.

Molecularly imprinting technology (MIT) is well-known for designing and preparing molecularly imprinted polymers (MIPs) with man-made cavities matched with target in shape, dimension and binding sites, enabling the MIPs to specifically recognize the target in complex systems [18,19]. Typically, the functional monomer is initially interacted with the template molecule to form a host-guest complex, after which a cross-linker captures the complex to form stereoscopic polymers via free radical polymerization. Finally, removal of the template from the polymers yields the designed MIPs with specific cavities. So far, a few attempts combining MIPs and 2D COFs have already been applied in the selective adsorption of cyanidin-3-O-glucoside, enrofloxacin, UO_2^{2+} and others [20–24]. However, the engineering of molecularly imprinted cavities within 3D COFs has not yet been reported.

Herein, we aim to engineer molecularly imprinted cavities within 3D COFs via MIT to obtain a novel adsorbent with great selectivity, kinetics and capacity for the efficient extraction and removal of MCs. A new C═C bond-containing 3D COF, designated JNU-7, was synthesized through the condensation of tetrakis(4-aminophenyl)methane (TAM) and 1,4-benzenedicarboxaldehyde,2,5-bis(2-propen-1-yloxy) (BATA). Subsequently, JNU-7 and methacrylic acid (MAA), serving as functional buildings, were first interacted with the pseudo template of L-arginine to form a ternary complex. Ethylene dimethacrylate (EGDMA) was further applied as a cross-linker to stabilize the conformation of the complex. The 3D COF based MIP (JNU-7-MIP) with specific imprinted cavities was finally obtained upon the removal of L-arginine. The extraction and removal capabilities of JNU-7-MIP for MC-LR were systematically investigated in various environmental water samples.

2. Materials and methods

2.1. Materials and chemicals

Unless otherwise noted, all reagents are analytical grade. MC-LR and MC-RR (HPLC) were purchased from ANPEL Laboratory Technologies Co., Ltd. (Shanghai, China). L-arginine, humic acid (HA, Fulvic acid ≥ 90%), sulfamethoxazole (SMX, HPLC), and tetracycline (TC, HPLC) were bought from Macklin Biochemical Co., Ltd. (Shanghai, China). TAM and BATA were purchased from Jilin Chinese Academy of Sciences-Yanshen Technology Co., Ltd. (Jilin, China). Activated carbon (≥200 mesh), MAA, EGDMA, 2,2′-azobis(2-methylpropionitrile) (AIBN), 1,2-dichlorobenzene, tetrahydrofuran, NaOH, HCl, acetonitrile (ACN), formic acid, trifluoroacetic acid (TFA), n-butanol, acetic acid (HAc), ethanol (EtOH) and methanol (MeOH) were obtained from Aladdin Chemistry Co., Ltd. (Shanghai, China). Ultrapure water from Wahaha Co., Ltd. (Hangzhou, China) was used throughout this work. Ethylene diamine tetraacetic acid (EDTA) and $Na_4P_2O_7$ were purchased from Titan Technology Co., Ltd. (Shanghai, China). 0.22 μm membrane was bought from Agilent Technologies Co., Ltd. (Shanghai, China).

2.2. Synthesis of JNU-7

Typically, TAM (38.05 mg, 0.1 mmol) and BATA (49.25 mg, 0.2 mmol) were dissolved with mixed solution of 1,2-dichlorobenzene (0.2 mL), n-butanol (1.8 mL), and 6 M HAc (0.4 mL) in a pyrex tube, sonicated for 30 min, degassed by three cycles of freeze-pump-thaw, then reacted in an oil bath at 120 °C for 3 days. The obtained yellow solid product was collected with centrifugation and exhaustively washed with tetrahydrofuran and dried under vacuum at 60 °C overnight to obtain JNU-7 (yield, ca.82.1%).

2.3. Synthesis of JNU-7-MIP

The JNU-7-MIP was synthesized referring to some previous works [25,26]. The mixture of JNU-7 (15.0 mg), L-arginine (17.4 mg), ACN (10 mL) and TFA (40 μL) was added into a three-necked round-bottomed flask, stirred for 20 min. Next, MAA (68 μL, 0.8 mmol) and EGDMA (189 μL, 1.0 mmol) were added into the mixture and further stirred for 20 min. Finally, AIBN (20.0 mg) was added and sonicated for 10 min. The final mixture was deoxygenated by purging nitrogen for 10 min and then stirred at 60 °C for 24 h. The resulting precipitate was washed with MeOH for three times, and further rinsed by Soxhlet extraction with MeOH and HAc (9:1, v/v) as eluent to remove template to obtain the JNU-7-MIP. In addition, JNU-7 based non-molecularly imprinted polymer (JNU-7-NIP) was synthesized with identical procedures as JNU-7-MIP except for no addition of L-arginine. The preparation of JNU-7 free MIP (bare MIP) was listed in SI.

2.4. Solid-phase extraction

Briefly, 10 mg of JNU-7-MIP was dispersed in 20 mL of MC-LR standard or sample solution (pH 4) with a specific concentration. After shaking for 10 min, the JNU-7-MIP was collected by centrifugation and subsequently eluted with 1 mL mixture of MeOH and HAc (9:1, v/v). The collected eluate was filtered with a 0.22 μm membrane, dried with nitrogen and then dissolved in 0.1 mL MeOH for LC-MS analysis.

2.5. Sample analysis

The soil samples were from the Taihu lake. According to the reported

method [27], the freeze-dried soil (2 g) was vortexed with 25 mL mixture of 0.1 M EDTA and $Na_4P_2O_7$ acidified with 0.1% TFA (v/v) for 60 s. After ultrasound for 30 min, the supernatant was collected by centrifugation at 10,000 rpm, then dried with nitrogen. The obtained residue was dissolved in 0.1 mL MeOH and made up to 20 mL with ultrapure water (pH 4) for subsequent solid-phase extraction (SPE) and analysis. 20 mL water samples from Lihu and Taihu lake were filtered through a 0.22 μm membrane, adjusted the pH to 4 with 0.1 M HCl for subsequent SPE and analysis.

2.6. Removal

Typically, 1 mg of JNU-7-MIP was dispersed in 1 mL of samples and then shaken at 150 rpm for 30 min. The supernatant was collected with filter, and then analyzed with our developed method for determination of MC-LR. Removal rate of MC-LR was calculated by the following formula:

$$\text{Removal rate } (\%) = \frac{C_0 - C_1}{C_0} \times 100\%$$

where C_0 and C_1 are the concentrations of MC-LR before and after the adsorption with JNU-7-MIP, respectively.

3. Result and discussion

3.1. Preparation and characterization of JNU-7

The molecularly imprinted cavity is conventionally formed via free radical polymerization. Accordingly, a new C═C bond-containing 3D COF is required for the subsequent engineering of molecularly imprinted cavities. TAM, with its symmetrical tetrahedral structure crucial for the formation of a 3D structure, was selected to react with C═C bond-containing monomer BATA, yielding the new 3D COF JNU-7 (Fig. 1). The prepared COF appeared characteristic PXRD peaks at 7.7°, 15.5°, 21.0° and 23.0°, which is coincidence with the simulated PXRD patterns of JNU-7 with a dia-7 structure. Pawley refinement of the experimental PXRD data (Rp = 4.76%, Rwp = 6.38%) revealed the specific structure of JNU-7 with unit cell parameters of space group I41/A (a = b = 24.1827 Å, c = 12.9849 Å, and α = β = γ = 90°) (Fig. 2a and Table S1). Appearance of an FTIR peak at 1615 cm^{-1}, attributing to stretching vibration of the C═N bond, indicates the condensation of TAM and BATA. Furthermore, the peak at 1485 cm^{-1} verifies the presence of C═C bonds in JNU-7 (Fig. 2b).

The Brunauer-Emmett-Teller (BET) surface area, pore volume and pore size of JNU-7 calculated from the N_2 adsorption experiment were found to be 762.2 m^2 g^{-1}, 0.59 cm^3 g^{-1}, and 10.6 Å, respectively (Fig. 2c and S1). These results highlight that JNU-7 has a large BET surface area along with porous structure, which confers plentiful accessible active sites to interact with analytes. Scanning electron micrographs show that JNU-7 exhibits a morphology of bar-shaped

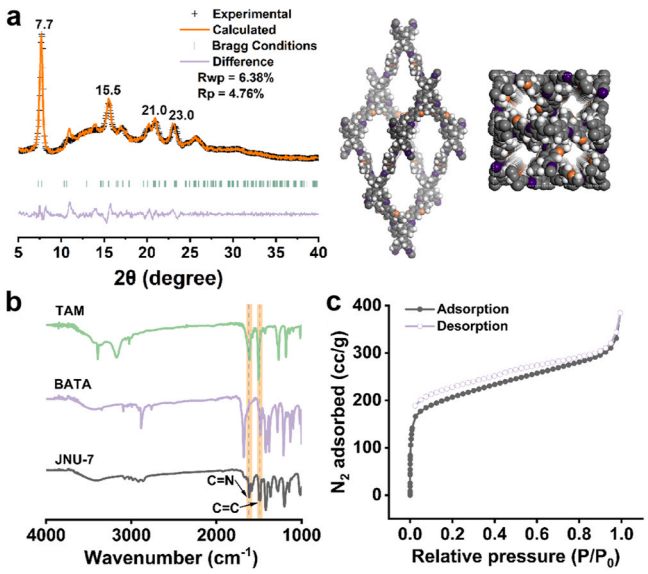

Fig. 2. (a) Experimental and simulated PXRD patterns, structural representation of crystal unit of JNU-7 (gray C, white H, purple N, orange O). (b) FT-IR spectra of TAM, BATA and JNU-7. (c) N_2 adsorption-desorption isotherms of JNU-7.

aggregation (Fig. S2). No significant change in the PXRD patterns and FTIR spectra of JNU-7 after immersing in ACN, MeOH, THF, H_2O and 0.1 M HCl proves the high chemical stability of JNU-7 (Fig. S3 and S4).

3.2. Preparation and characterization of JNU-7-MIP

High toxicity and cost of MC-LR render it impractical to function directly as template. Instead, L-arginine is suitable to serve as pseudo template due to the existence of an L-arginine-like structure in the relevant MC-LR congeners [28] (Fig. S5). MAA was employed as additional functional monomer. EGDMA was used as a cross-linker due to its strong copolymerization capabilities via free radical polymerization. High selectivity and adsorption ability for the target molecule play key roles for an excellent adsorbent. Hence, the amounts of JNU-7, L-arginine, MAA, and EGDMA, as well as polymerization time and temperature, were optimized using adsorption capacity (q) and imprinting factor (IF) as performance indicators to ensure the excellent adsorption ability and selectivity of the prepared 3D COF MIP for the target MCs.

Although the q improved with the increase of JNU-7, the IF decreased when more than 15 mg JNU-7 was added (Fig. S6). The IF promoted as the MAA rose from 0.4 to 0.8 mmol. Further increasing MAA led to a decline in both q and IF (Fig. S7), resulting from the increased non-specific interactions [29]. Similarly, the q of JNU-7-MIP and JNU-7-NIP promoted as EGDMA increased from 0.5 to 1.0 mmol, but then significantly declined after addition of more than 1.0 mmol

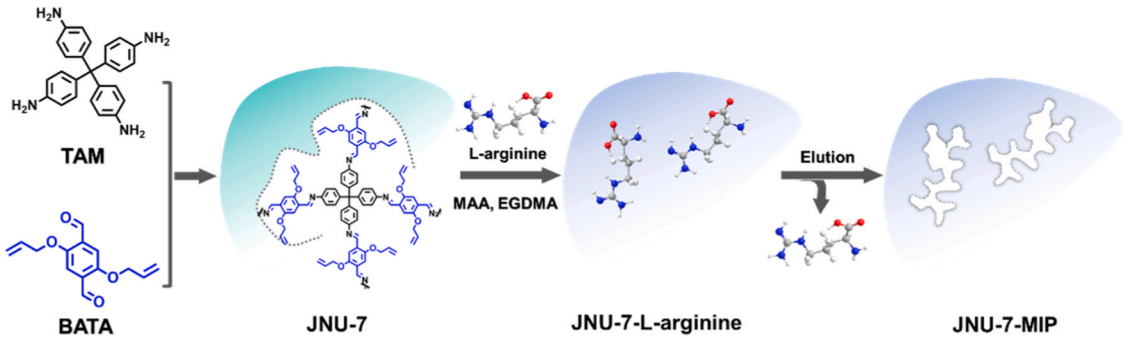

Fig. 1. Schematic for the preparation of JNU-7 and JNU-7-MIP.

EGDMA (Fig. S8). The EGDMA profits the formation of imprinted cavities, but excessive EGDMA would block the cavities [21]. Accordingly, 15 mg of JNU-7, 0.8 mmol of MAA and 1.0 mmol of EGDMA were applied for the preparation of JNU-7-MIP.

The polymerization time ranging from 12 to 24 h evidently improved the IF of JNU-7-MIP. Further increasing the polymerization time caused a decline in IF (Fig. S9), likely resulting from increased polymer thickness [30]. The effect of temperature on the IF demonstrated that the highest IF was obtained at 60 °C (Fig. S10). Because rapid polymerization rate at high temperature favors the formation of non-imprinted self-polymer of the cross-linker over imprinted cavities [31], while the decreased catalytic efficiency of AIBN at low temperature (< 50 °C) negatively impacts the polymerization.

The PXRD patterns of JNU-7-MIP displayed a distinct JNU-7 characteristic peak at 7.7°, indicative of the presence of a crystal structure (Fig. 3a). The appearance of C═O (1725 cm^{-1}) and C═N (1615 cm^{-1}) in the FT-IR spectrum of JNU-7-MIP, confirmed the successful formation of imprinted polymers (Fig. 3b). JNU-7-MIP gave a more spherical morphology in contrast to JNU-7, attributing to the polymerization of the cross-linker (Fig. S11). The BET surface area of JNU-7-MIP was calculated to be 504.5 $m^2\ g^{-1}$ (Fig. 3c), lower than that of JNU-7 due to the introduction of the imprinted polymer. Furthermore, JNU-7-MIP showed an additional narrow pore size distribution centered around 5.2 Å and a larger pore volume (1.0 $cm^3\ g^{-1}$) compared to JNU-7 (Fig. 3d), substantiating the formation of imprinted cavities. The large surface area and ordered crystal structure of JNU-7-MIP would enhance the accessibility of imprinted sites to target. No significant changes in the PXRD patterns of JNU-7-MIP after immersion in ACN, MeOH, THF, H_2O and 0.1 M HCl proved that JNU-7-MIP still maintained its certain crystal form (Fig. S12). Likewise, the retention of FT-IR spectra indicates no compositional change in JNU-7-MIP (Fig. S13). Moreover, the JNU-7-NIP was also prepared and characterized as a control to demonstrate the successful preparation of JNU-7-MIP (Fig. 3 and S14).

3.3. Optimization of JNU-7-MIP based SPE

The extraction rate of MC-LR improved with increasing amounts of JNU-7-MIP, and remained unchanged when 10 mg JNU-7-MIP was used in the extraction (Fig. 4a). The extraction rate of MC-LR was stable after 10 min, indicating the complete extraction in 10 min (Fig. 4b). The rapid extraction kinetics of JNU-7-MIP for MC-LR can be attributed to the ordered porous structure. Increasing pH from 2 to 4 led to a promotion in extraction rate from 77% to 93%. Further increases in pH did not significantly improve extraction rate , demonstrating the favorability of pH 4 for extraction (Fig. 4c). The eluent type, eluent volume and elution time were also optimized with extraction rate as the performance indicator. The results revealed eluting with 1 mL MeOH/HAc (9/1,v/v) for 10 min was sufficient for the complete desorption of MC-LR from JNU-7-MIP (Fig. 4d–f).

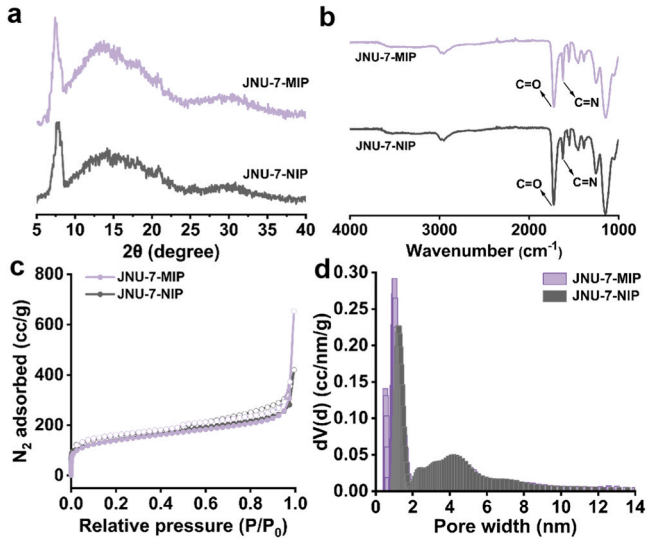

Fig. 3. (a) PXRD patterns, (b) FT-IR spectra, (c) N_2 adsorption-desorption isotherms, and (d) pore size distribution of JNU-7-MIP and JNU-7-NIP.

3.4. Analytical performance

The prepared JNU-7-MIP demonstrated an enrichment factor of 186 for MC-LR (Table S2). A JNU-7-MIP based SPE coupled with HPLC-MS method was established for the precise determination of MC-LR. The developed JNU-7-MIP SPE-HPLC-MS method exhibited excellent linearity ($R^2 > 0.9999$) in a wide concentration range of 0.025–100 ng mL^{-1} (Fig. S15). The limit of detection (LOD, S/N = 3), and limit of quantification (LOQ, S/N = 10) of the proposed method were calculated to be 0.008 and 0.025 ng mL^{-1}, respectively. The intraday (1.9%), interday (3.6%) and inter-batch (4.8%) relative standard deviations (RSD) of the extraction rate (n = 6) were all lower than 5%, indicating good reproducibility of JNU-7-MIP. The developed method exhibited faster extraction, wider linearity and lower LOD than various reported methods (Table S3).

Antibiotics such as SMZ and TC facilitate formation of cyanobacterial bloom in eutrophic lake water [32], thereby serving as major disruptors in the detection of MCs. The extraction rate of JNU-7-MIP for MC-LR still remained above 90% despite the presence of SMZ and TC (1 μg mL^{-1}) at a concentration 100 times higher than that of MC-LR, indicating the excellent selectivity of JNU-7-MIP (Fig. 5a). The extraction rate of MC-LR on JNU-7-MIP gave little decrease to above 80% after 10 extraction cycles, mainly due to swelling deformation of the imprinted polymer [20]. In contrast, the extraction rate of bare MIP for MC-LR dropped below 60% under the same conditions (Fig. S16), highlighting the positive effect of JNU-7 in promotion of the stability.

3.5. Mechanism

JNU-7-MIP exhibited a higher extraction rate for MC-LR (92.3%) than bare MIP (51.4%) (Fig. 5b). Both JNU-7-MIP and JNU-7-NIP required shorter extraction times than bare MIP, indicating the benefit of the ordered structure of JNU-7 in enhancing mass transfer efficiency and extraction performance (Fig. S17). The q of MC-LR on JNU-7-MIP were 3.1 times higher than that of JNU-7-NIP, whereas JNU-7-MIP showed no appreciable difference from JNU-7-NIP in adsorption of SMZ and TC. In addition, JNU-7-MIP also displayed a higher q for other MCs containing an L-arginine structure, such as MC-RR, than JNU-7-NIP, confirming the dominance of imprinted cavities for the adsorption (Fig. S5 and S18).

In addition to the structural complementarity, the interaction forces between the imprinted cavities and template are crucial for selective recognition. The MC-LR adsorbed JNU-7-MIP gave a red shift in the fluorescence characteristic peak of the carbonyl group at 426 nm (Fig. S19). The C═O stretching peak in FTIR spectra of JNU-7-MIP also shifted from 1724 cm^{-1} to 1728 cm^{-1}, demonstrating the hydrogen bonding interactions between JNU-7-MIP and MC-LR (Fig. S20) [33–35]. Moreover, the zeta potential of JNU-7-MIP at the range of pH 2 to 9 showed a change from positive to negative at pH 5.4, proving the accessible protonation of JNU-7-MIP at pH 4 (Fig. S21). The dominant species of MC-LR is negative [$(COO\text{-})_2(NH_2^+)$] when pH > 2.19 [36], indicating the involvement of electrostatic interaction in the specific recognition of MC-LR.

3.6. Real sample analysis

The developed JNU-7-MIP SPE-HPLC-MS method was applied to analyze MC-LR in real water and soil collected from Taihu and Lihu

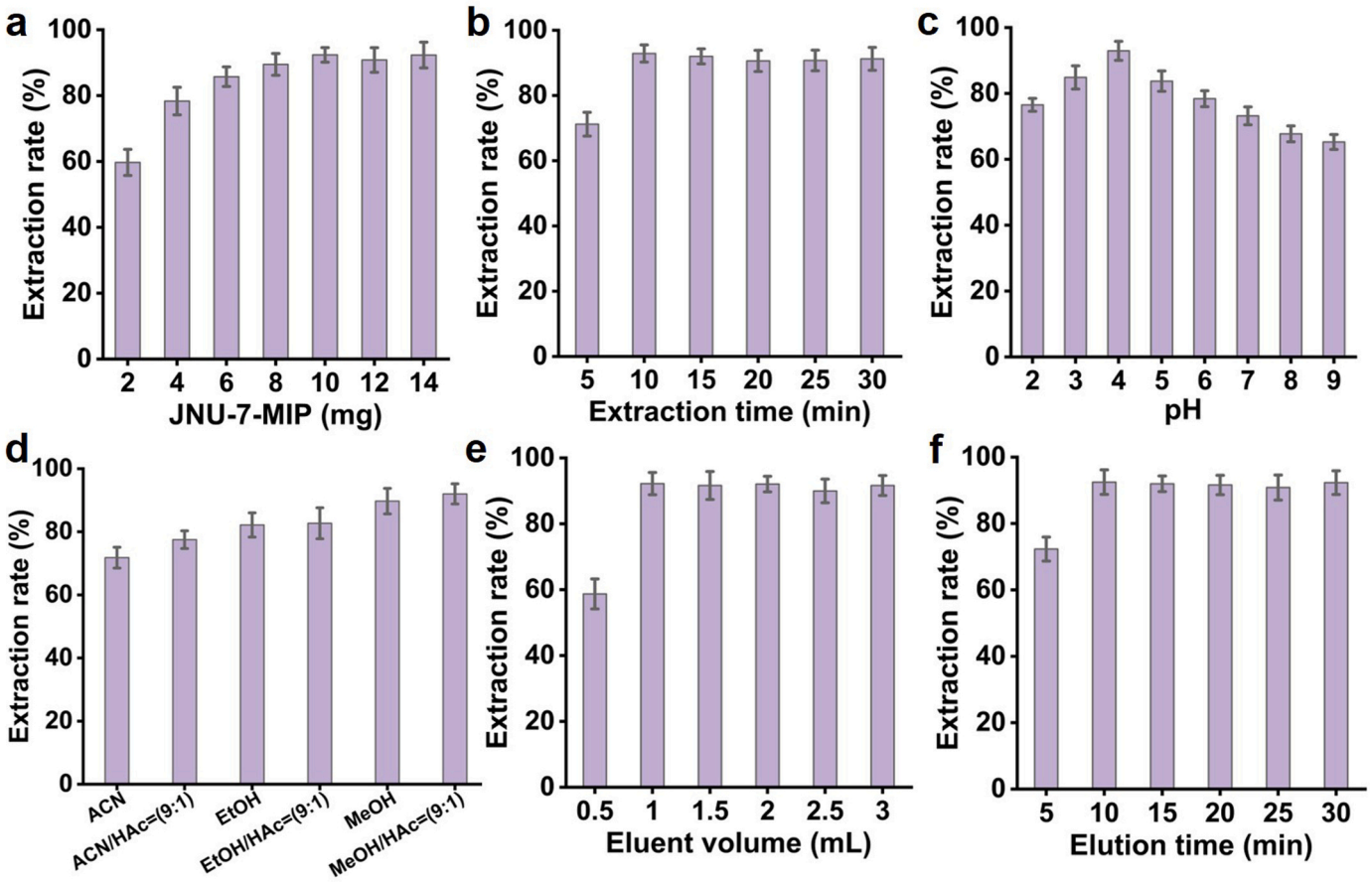

Fig. 4. Effect of (a) amounts of JNU-7-MIP, (b) extraction time, (c) pH, (d) eluent type, (e) eluent volume and (f) elution time on the extraction rate of MC-LR. All fixed parameters were set at their respective optimal levels during the optimization of variables. Sample volume at 20 mL, MC-LR at 10 μg L^{-1}.

lakes. Compared with original Taihu lake sample, the sample after extraction with JNU-7-MIP gave an evident peak of MC-LR in the chromatograms, evidencing the strong enrichment ability of JNU-7-MIP (Fig. 5c). The matrix effect (%ME) for the real samples ranged from 5.12% to 7.48% (Table S4), demonstrating the great selectivity and matrix removal property of the prepare JNU-7-MIP[37]. MC-LR was detected in water (0.44 ng mL^{-1}) and soil (0.23 ng g^{-1}) from Taihu lake, whereas no detectable levels were found in water from Lihu lake. The recoveries of spiked samples fell within the range from 92.4% to 106.5% (Table 1). Moreover, the detection results of MC-LR (spiked at 20 ng g^{-1}) showed no statistically significant differences ($P > 0.05$) between our method and EPA recommended method (Fig. S22), indicating the accuracy of the proposed JNU-7-MIP SPE-HPLC-MS.

3.7. Removal of MC-LR

The higher adsorption capacity (156 mg g^{-1}) and more rapid adsorption equilibrium (20 min) of JNU-7-MIP than JNU-7-NIP for the pseudo template of L-arginine not only indicate the key roles of specific imprinted cavities in the adsorption, but also inspire us to explore the removal capability of JNU-7-MIP for MC-LR (Fig. S23 and S24). The JNU-7-MIP achieved remarkable removal rate of 99.9% and 99.1% when the initial concentration of MC-LR were 1 and 6 mg L^{-1}, respectively (Fig. S25). The removal rate of JNU-7-MIP was evidently higher than that of bare MIP, attributing to the incorporation of the ordered JNU-7 with large BET surface area (Fig. S26). Furthermore, the JNU-7-MIP can rapidly decrease the concentration of MC-LR from 1 mg L^{-1} to 0.26 (ultrapure water), 0.29 (Lihu lake), and 0.35 μg L^{-1} (Taihu lake) within 30 min, all of which are lower than the WHO recommended limit for drinking water of 1 μg L^{-1} (Table S5). The preservation of PXRD patterns and FT-IR spectra indicates the structure stability of JNU-7-MIP during the removal (Fig. S27 and S28).

As activated carbon is the most widely applied adsorbent at technical scale, the comparison of the JNU-7-MIP and activated carbon in adsorption of MC-LR was investigated. The JNU-7-MIP can complete the removal within 30 min, less than the time taken by activated carbon (120 min) (Fig. S29). Although the removal rate of activated carbon for MC-LR was slightly higher than that of JNU-7-MIP in pure water, the presence of interfering substances significantly reduced the removal rate of activated carbon for MC-LR from 94.3% to 58.7%, whereas it gave no obvious impact on JNU-7-MIP, due to the non-specific adsorption of activated carbon (Fig. S30). Moreover, when contrasted with numerous reported adsorbents, JNU-7-MIP also excelled in MC-LR removal (Fig. 5d) [38–43], demonstrating its excellent potential as a candidate for purification of water heavily contaminated with MCs.

4. Conclusion

In short, we have prepared a new 3D COF-MIP as novel adsorbent for the extraction and removal of MCs in environmental samples. The combination of 3D COF with large specific surface area and highly ordered rigid structure, and specific imprinted cavities renders 3D COF-MIP with high selectivity and fast adsorption kinetics for target MCs. Consequently, the 3D-MIP based analytical method exhibits rapid and precise detection of MCs in environmental samples. Furthermore, the high adsorption capacity of the proposed 3D COF-MIP can effectively remove massive MCs from real water samples, highlighting the considerable potential of 3D COF-MIP in both detection and control of

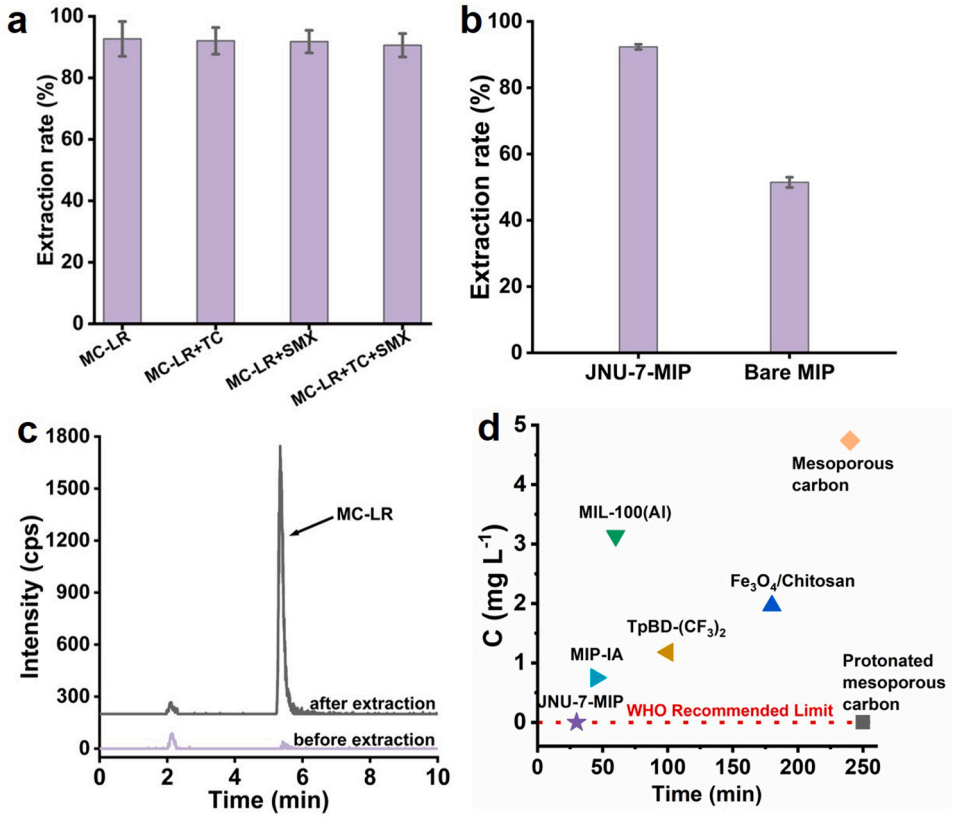

Fig. 5. (a) Effect of TC and SMX (1 μg mL^{-1}) on the extraction rate of JNU-7-MIP for MC-LR (10 ng mL^{-1}). (b) Extraction rate of MC-LR (1 mg L^{-1}) on JNU-7-MIP and bare MIP. (c) Chromatograms of water sample spiked with 2 ng mL^{-1} MC-LR before and after extraction with JNU-7-MIP. (d) Comparison of time and residual concentration among JNU-7-MIP and other reported adsorbents for removing MC-LR. Concentration of adsorbents in removal: JNU-7-MIP, MIL-100(Al) and TpBD-$(CF_3)_2$ at 1 mg mL^{-1}; Fe_3O_4/Chitosan at 25 mg mL^{-1}; mesoporous carbon at 0.01 mg mL^{-1}; protonated mesoporous carbon at 0.1 mg mL^{-1}; itaconic acid molecularly imprinted polymer (MIP-IA) at 10 mg mL^{-1}.

Table 1
Analytical results for the determination of MC-LR in water and soil sample (n = 6).

Sample	Spiked MC-LR (ng mL^{-1}/ng g^{-1})	JNU-7-MIP	
		Concentration determined (ng mL^{-1}/ng g^{-1})	Recovery (%)
Lihu lake	0	ND[a]	-
	0.8	0.77 ± 0.03	95.9 ± 4.1
	2.0	1.99 ± 0.05	99.6 ± 2.4
	20	19.75 ± 0.45	98.8 ± 2.3
	80	76.35 ± 2.69	95.4 ± 3.4
Taihu lake	0	0.44 ± 0.02	-
	0.8	1.23 ± 0.06	98.9 ± 4.9
	2.0	2.35 ± 0.09	96.4 ± 3.9
	20	19.84 ± 0.40	97.1 ± 2.0
	80	74.32 ± 2.60	92.4 ± 3.2
Taihu soil	0	0.23 ± 0.02	-
	0.8	1.03 ± 0.05	100.2 ± 4.7
	2.0	2.22 ± 0.05	99.5 ± 2.1
	20	21.55 ± 0.72	106.5 ± 3.6
	80	83.30 ± 2.52	103.8 ± 3.1

[a] not detected

contaminants in real samples.

Environmental implication

Global warming and man-made eutrophication have greatly raised the hazardous exposure levels of microcystins (MCs) in environment. The scarcity of selective adsorbents capable of efficiently extracting and removing MCs from complex samples severely limits the precise detection and effective control of MCs. Here, a new molecularly imprinted three-dimensional covalent organic framework was designed and prepared as novel adsorbent for the efficient extraction and remove of MCs in real environmental samples.

CRediT authorship contribution statement

Xu-Qin Ran: Methodology. **Yukun Yang:** Methodology. **Yu-Hong Tang:** Writing – original draft, Methodology, Data curation. **Tian-Tian Ma:** Methodology. **Hai-Long Qian:** Writing – review & editing, Supervision, Funding acquisition, Conceptualization. **Xiu-Ping Yan:** Writing – review & editing, Resources.

Declaration of Competing Interest

The authors declare that they have no known competing financial interests or personal relationships that could have appeared to influence the work reported in this paper.

Data Availability

Data will be made available on request.

Acknowledgments

This work was supported by the National Natural Science Foundation of China (nos. 22076066, 22376082 and 22176073), Jiangsu Funding Program for Excellent Postdoctoral Talent (No. 2023ZB116), Youth

Program of Nature Science Foundation of Shandong Province, and the "Fundamental Research Funds for the Central Universities".

Appendix A. Supporting information

Supplementary data associated with this article can be found in the online version at doi:10.1016/j.jhazmat.2024.134469.

References

[1] Svirčev, Z., Lalić, D., Bojadžija Savić, G., Tokodi, N., Drobac Backović, D., Chen, L., Meriluoto, J., Codd, G.A., 2019. Global geographical and historical overview of cyanotoxin distribution and cyanobacterial poisonings. Arch Toxicol 93 (9), 2429–2481. https://doi.org/10.1007/s00204-019-02524-4.

[2] Shi, L., Du, X., Liu, H., Chen, X., Ma, Y., Wang, R., Tian, Z., Zhang, S., Guo, H., Zhang, H., 2021. Update on the adverse effects of microcystins on the liver. Environ Res 195, 110890. https://doi.org/10.1016/j.envres.2021.110890.

[3] McCarty, C.L., Nelson, L., Eitniear, S., Zgodzinski, E., Zabala, A., Billing, L., DiOrio, M., 2016. Community needs assessment after microcystin toxin contamination of a municipal water supply - Lucas county, Ohio, September 2014. Morb Mortal Wkly Rep 65 (35), 925–929. https://doi.org/10.15585/mmwr.mm6535a1.

[4] Falconer, I.R., Beresford, A.M., Runnegar, M.T., 1983. Evidence of liver damage by toxin from a bloom of the blue-green alga, Microcystis aeruginosa. Med J Aust 1 (11), 511–514. https://doi.org/10.5694/j.1326-5377.1983.tb136192.x.

[5] Zurawell, R.W., Chen, H., Burke, J.M., Prepas, E.E., 2005. Hepatotoxic cyanobacteria: a review of the biological importance of microcystins in freshwater environments. J Toxicol Environ Health B Crit Rev 8 (1), 1–37. https://doi.org/10.1080/10937400590889412.

[6] Redouane, E.M., El Amrani Zerrifi, S., El Khalloufi, F., Oufdou, K., Oudra, B., Lahrouni, M., Campos, A., Vasconcelos, V., 2019. Mode of action and fate of microcystins in the complex soil-plant ecosystems. Chemosphere 225, 270–281. https://doi.org/10.1016/j.chemosphere.2019.03.008.

[7] Massey, I.Y., Yang, F., Ding, Z., Yang, S., Guo, J., Tezi, C., Al-Osman, M., Kamegni, R.B., Zeng, W., 2018. Exposure routes and health effects of microcystins on animals and humans: a mini-review. Toxicon 151, 156–162. https://doi.org/10.1016/j.toxicon.2018.07.010.

[8] Ibelings, B.W., Backer, L.C., Kardinaal, W.E.A., Chorus, I., 2014. Current approaches to cyanotoxin risk assessment and risk management around the globe. Harmful Algae 40, 63–74. https://doi.org/10.1016/j.hal.2014.10.002.

[9] Pichon, V., Delaunay, N., Combès, A., 2020. Sample preparation using molecularly imprinted polymers. Anal Chem 92 (1), 16–33. https://doi.org/10.1021/acs.analchem.9b04816.

[10] Pan, S.-D., Chen, X.-H., Li, X.-P., Cai, M.-Q., Shen, H.-Y., Zhao, Y.-G., Jin, M.-C., 2015. Double-sided magnetic molecularly imprinted polymer modified graphene oxide for highly efficient enrichment and fast detection of trace-level microcystins from large-volume water samples combined with liquid chromatography-tandem mass spectrometry. J Chromatogr A 1422, 1–12. https://doi.org/10.1016/j.chroma.2015.10.007.

[11] Sharma, R.K., Yadav, P., Yadav, M., Gupta, R., Rana, P., Srivastava, A., Zbořil, R., Varma, R.S., Antonietti, M., Gawande, M.B., 2020. Recent development of covalent organic frameworks (COFs): synthesis and catalytic (organic-electro-photo) applications. Mater Horiz 7 (2), 411–454. https://doi.org/10.1039/C9MH00856J.

[12] Geng, K., He, T., Liu, R., Dalapati, S., Tan, K.T., Li, Z., Tao, S., Gong, Y., Jiang, Q., Jiang, D., 2020. Covalent organic frameworks: design, synthesis, and functions. Chem Rev 120 (16), 8814–8933. https://doi.org/10.1021/acs.chemrev.9b00550.

[13] Wang, Z., Zhang, S., Chen, Y., Zhang, Z., Ma, S., 2020. Covalent organic frameworks for separation applications. Chem Soc Rev 49 (3), 708–735. https://doi.org/10.1039/C9CS00827F.

[14] Song, Y., Sun, Q., Aguila, B., Ma, S., 2019. Opportunities of covalent organic frameworks for advanced applications. Adv Sci 6 (2), 1801410. https://doi.org/10.1002/advs.201801410.

[15] Huang, N., Wang, P., Jiang, D., 2016. Covalent organic frameworks: a materials platform for structural and functional designs. Nat Rev Mater 1 (10), 16068. https://doi.org/10.1038/natrevmats.2016.68.

[16] Gui, B., Lin, G., Ding, H., Gao, C., Mal, A., Wang, C., 2020. Three-dimensional covalent organic frameworks: from topology design to applications. Acc Chem Res 53 (10), 2225–2234. https://doi.org/10.1021/acs.accounts.0c00357.

[17] Guan, X., Chen, F., Fang, Q., Qiu, S., 2020. Design and applications of three dimensional covalent organic frameworks. Chem Soc Rev 49 (5), 1357–1384. https://doi.org/10.1039/C9CS00911F.

[18] Gerente, C., Lee, V.K.C., Cloirec, P.L., McKay, G., 2007. Application of chitosan for the removal of metals from wastewaters by adsorption-mechanisms and models review. Crit Rev Environ Sci Technol 37 (1), 41–127. https://doi.org/10.1080/10643380600729089.

[19] Yan, H., Row, K.H., 2006. Characteristic and synthetic approach of molecularly imprinted polymer. Int J Mol Sci 7 (5), 155–178. https://doi.org/10.3390/i7050155.

[20] Zhao, Q., Zhang, H., Zhao, H., Liu, J., Liu, J., Chen, Z., Li, B., Liao, X., Regenstein, J.M., Wang, J., Yang, X., 2020. Strategy of fusion covalent organic frameworks and molecularly imprinted polymers: a surprising effect in recognition and loading of cyanidin-3-o-glucoside. ACS Appl Mater Interfaces 12 (7), 8751–8760. https://doi.org/10.1021/acsami.9b21460.

[21] Su, L.H., Qian, H.L., Yang, C., Wang, C., Wang, Z., Yan, X.P., 2023. Surface imprinted-covalent organic frameworks for efficient solid-phase extraction of fluoroquinolones in food samples. J Hazard Mater 459, 132031. https://doi.org/10.1016/j.jhazmat.2023.132031.

[22] Wang, J., Sang, Y., Liu, W., Liang, N., Wang, X., 2017. The development of a biomimetic enzyme-linked immunosorbent assay based on the molecular imprinting technique for the detection of enrofloxacin in animal-based food. Anal Methods 9 (47), 6682–6688. https://doi.org/10.1039/c7ay02321a.

[23] Yuan, Y., Yang, Y., Ma, X., Meng, Q., Wang, L., Zhao, S., Zhu, G., 2018. Molecularly imprinted porous aromatic frameworks and their composite components for selective extraction of uranium ions. Adv Mater 30 (12), e1706507. https://doi.org/10.1002/adma.201706507.

[24] Singh, D.K., Mishra, S., 2009. Synthesis and characterization of UO_2^{2+}-ion imprinted polymer for selective extraction of UO_2^{2+}. Anal Chim Acta 644 (1-2), 42–47. https://doi.org/10.1016/j.aca.2009.04.020.

[25] Li, C.Y., Lv, S.W., Yang, L., Wang, J., Liu, J.M., Wang, S., 2022. Facile preparation of uniform-sized covalent organic framework nanoflowers as versatile sample-pretreatment platforms for sensitive and specific determination of hazardous substances. J Hazard Mater 438, 129566. https://doi.org/10.1016/j.jhazmat.2022.129566.

[26] Han, L., Meng, C., Zhang, D., Liu, H., Sun, B., 2022. Fabrication of a fluorescence probe via molecularly imprinted polymers on carbazole-based covalent organic frameworks for optosensing of ethyl carbamate in fermented alcoholic beverages. Anal Chim Acta 1192, 339381. https://doi.org/10.1016/j.aca.2021.339381.

[27] Chen, W., Li, L., Gan, N., Song, L., 2006. Optimization of an effective extraction procedure for the analysis of microcystins in soils and lake sediments. Environ Pollut 143 (2), 241–246. https://doi.org/10.1016/j.envpol.2005.11.030.

[28] Hitzfeld, B.C., Höger, S.J., Dietrich, D.R., 2000. Cyanobacterial toxins: removal during drinking water treatment, and human risk assessment. Environ Health Perspect 108 (suppl 1), 113–122. https://doi.org/10.1289/ehp.00108s1113.

[29] Rachkov, A., Minoura, N., 2000. Recognition of oxytocin and oxytocin-related peptides in aqueous media using a molecularly imprinted polymer synthesized by the epitope approach. J Chromatogr A 889 (1), 111–118. https://doi.org/10.1016/S0021-9673(00)00568-9.

[30] Pan, S.D., Chen, X.H., Li, X.P., Cai, M.Q., Shen, H.Y., Zhao, Y.G., Jin, M.C., 2015. In situ controllable synthesis of graphene oxide-based ternary magnetic molecularly imprinted polymer hybrid for efficient enrichment and detection of eight microcystins. J Mater Chem A 3 (45), 23042–23052. https://doi.org/10.1039/c5ta05840f.

[31] Ou, J., Li, X., Feng, S., Dong, J., Dong, X., Kong, L., Ye, M., Zou, H., 2007. Preparation and evaluation of a molecularly imprinted polymer derivatized silica monolithic column for capillary electrochromatography and capillary liquid chromatography. Anal Chem 79 (2), 639–646. https://doi.org/10.1021/ac061475x.

[32] Xu, S., Jiang, Y., Liu, Y., Zhang, J., 2021. Antibiotic-accelerated cyanobacterial growth and aquatic community succession towards the formation of cyanobacterial bloom in eutrophic lake water. Environ Pollut 290, 118057. https://doi.org/10.1016/j.envpol.2021.118057.

[33] Zhong, X., Lu, Z., Liang, W., Hu, B., 2020. The magnetic covalent organic framework as a platform for high-performance extraction of Cr(VI) and bisphenol a from aqueous solution. J Hazard Mater 393, 122353. https://doi.org/10.1016/j.jhazmat.2020.122353.

[34] Zhang, Y., Li, Y., Zhang, L., 2021. Fabricating multifunctional low-toxicity ratiometric fluorescent probe for individual detection of Cu^{2+}/glutamate and continuous sensing for glutamate via Cu^{2+}-based platform. Spectrochim Acta A Mol Biomol Spectrosc 259, 119892. https://doi.org/10.1016/j.saa.2021.119892.

[35] Liu, B.L., Li, Y.W., Xie, L.S., Guo, J.J., Xiang, L., Mo, C.H., 2022. Sorption of microcystin-RR onto surface soils: characteristics and influencing factors. J Hazard Mater 431, 128571. https://doi.org/10.1016/j.jhazmat.2022.128571.

[36] De Maagd, P.J., hendriks, A., Seinen, W., Sijm, D., 1999. pH-dependent hydrophobicity of the cyanobacteria toxin microcystin-LR. Water Res 33 (3), 677–680. https://doi.org/10.1016/s0043-1354(98)00258-9.

[37] Pano-Farias, N.S., Ceballos-Magaña, S.G., Muñiz-Valencia, R., Gonzalez, J., 2017. Validation and assessment of matrix effect and uncertainty of a gas chromatography coupled to mass spectrometry method for pesticides in papaya and avocado samples. J Food Drug Anal 25 (3), 501–509. https://doi.org/10.1016/j.jfda.2016.09.005.

[38] He, Y., Wu, P., Li, G., Li, L., Yi, J., Wang, S., Lu, S., Ding, P., Chen, C., Pan, H., 2020. Optimization on preparation of Fe_3O_4/chitosan as potential matrix material for the removal of microcystin-LR and its evaluation of adsorption properties. Int J Biol Macromol 156, 1574–1583. https://doi.org/10.1016/j.ijbiomac.2019.11.209.

[39] Xia, W., Zhang, X., Xu, L., Wang, Y., Lin, J., Zou, R., 2013. Facile and economical synthesis of metal-organic framework MIL-100(Al) gels for high efficiency removal of microcystin-LR. Rsc Adv 3 (27). https://doi.org/10.1039/c3ra40741a.

[40] Teng, W., Wu, Z., Fan, J., Chen, H., Feng, D., Lv, Y., Wang, J., Asiri, A.M., Zhao, D., 2013. Ordered mesoporous carbons and their corresponding column for highly efficient removal of microcystin-LR. Energ Environ Sci 6 (9). https://doi.org/10.1039/c3ee41775a.

[41] Park, J.A., Kang, J.K., Jung, S.M., Choi, J.W., Lee, S.H., Yargeau, V., Kim, S.B., 2020. Investigating microcystin-LR adsorption mechanisms on mesoporous carbon, mesoporous silica, and their amino-functionalized form: surface chemistry, pore

structures, and molecular characteristics. Chemosphere 247, 125811. https://doi.org/10.1016/j.chemosphere.2020.125811.

[42] Fernandes, S.P.S., Kovář, P., Pšenička, M., Silva, A.M.S., Salonen, L.M., Espiña, B., 2021. Selection of covalent organic framework pore functionalities for differential adsorption of microcystin toxin analogues. ACS Appl Mater Interfaces 13 (13), 15053–15063. https://doi.org/10.1021/acsami.0c18808.

[43] Krupadam, R.J., Patel, G.P., Balasubramanian, R., 2012. Removal of cyanotoxins from surface water resources using reusable molecularly imprinted polymer adsorbents. Environ Sci Pollut R 19 (5), 1841–1851. https://doi.org/10.1007/s11356-011-0703-1.